

## **Paracrine Costimulation of IFN $\gamma$ Signaling by Integrins modulates CD8 T cell differentiation**

Matthew F. Krummel<sup>1\*§</sup>, Jagdish N. Mahale<sup>3§</sup>, Lion F.K. Uhl<sup>3</sup>, Emily A. Hardison<sup>1</sup>, Adriana M. Muijal<sup>1</sup>, Julie M. Mazet<sup>3</sup>, Robert J. Weber<sup>2</sup>, Zev J. Gartner<sup>2</sup>, and Audrey Gérard<sup>1,3\*</sup>

### **Affiliations:**

<sup>1</sup>Department of Pathology, University of California, San Francisco, 513 Parnassus Avenue, HSW512, San Francisco, CA 94143, USA

<sup>2</sup>Department of Pharmaceutical Chemistry, University of California, San Francisco, 600 16<sup>th</sup> Street, Box 2280, San Francisco, CA 94158, USA

<sup>3</sup>The Kennedy Institute of Rheumatology, University of Oxford, Roosevelt Dr., Oxford, OX3 7FY, UK

<sup>§</sup> Contributed equally

\*Correspondence: [audrey.gerard@kennedy.ox.ac.uk](mailto:audrey.gerard@kennedy.ox.ac.uk) or [matthew.krummel@ucsf.edu](mailto:matthew.krummel@ucsf.edu)

Classification: Biological Sciences, Immunology and Inflammation

Key words: cytokines, cell biology, T cell differentiation, integrins

## **Abstract**

The cytokine IFN $\gamma$  is a critical regulator of immune system development and function. Almost all leukocytes express the receptor for IFN $\gamma$ , yet each cell type elicits a different response to this cytokine. Cell type specific effects of IFN $\gamma$  make it difficult to predict the outcomes of the systemic IFN $\gamma$  blockade and limit its clinical application, despite many years of research. To better understand the cell-cell interactions and co-factors that specify IFN $\gamma$  functions, we focused on the function of IFN $\gamma$  on CD8 T cell differentiation. We demonstrated that during bacterial infection, IFN $\gamma$  is a dominant paracrine trigger that skews CD8 T cell differentiation towards memory. This skewing is preferentially driven by contact-dependent T cell-T cell interactions and the localized IFN $\gamma$  secretion amongst activated CD8 T cells in a unique splenic microenvironment and is less sensitive to concurrent IFN $\gamma$  production by other immune cell populations such as NK cells. Modulation of CD8 T cell differentiation by IFN $\gamma$  relies on non-conventional IFN $\gamma$  outcome which occurs specifically within 24 hours following infection. This is driven by IFN $\gamma$  costimulation by integrins at T cell-T cell synapses, and leads to synergistic phosphorylation of the proximal STAT1 molecule and accelerated Interleukin-2 receptor downregulation. This study provides novel evidence of the importance of context dependent cytokine signaling and gives another example of how cell clusters and microenvironment drive unique biology.

## **Significance Statement**

IFN $\gamma$  is one example of pleiotropic cytokines that plays critical roles in promoting both protective immune responses and immunopathologic processes. In response to this cytokine, cells activate a well-identified and conserved JAK/STAT signaling pathway that yet can elicit distinct responses, even in the same cell type. How this outcome specificity is achieved remains largely unknown. We have found that IFN $\gamma$  regulates CD8 T cell differentiation through non-canonical pathways that are enabled by integrin co-stimulation of the STAT1 pathway. This leads to cooperative effects between activating cell types that is dictated by proximity. This study demonstrates the importance of co-factors and microenvironment in eliciting specific cytokine functions.

\body

## Introduction

Interferon- $\gamma$  (IFN $\gamma$ ) is a pleiotropic cytokine potentially produced by all immune cells. It is crucial for immune responses against tumors (1) and infections (2), and is implicated in many autoimmune diseases (3). IFN $\gamma$  uses the same signaling machinery to elicit distinct and diverse responses (4). It consistently binds to a single receptor, composed of two chains, IFN $\gamma$ R1 and IFN $\gamma$ R2 (5) and triggers a conserved Janus kinases (JAKs) / Signal Transducer and Activator of Transcription 1 (STAT1) pathway (6). How specificity of IFN $\gamma$  action is achieved is still not understood. Differential expression of receptors and signaling components, leading to the integration of negative and positive feedbacks, have been described as a molecular basis of the cell specificity of cytokine action (7). But overall, deciphering the relevant microenvironment, cellular interactions and co-factors specifying the outcome of IFN $\gamma$  stimulation is still an outstanding question.

In CD8 T cells, IFN $\gamma$  production is traditionally associated with effector function and cytotoxicity . Interestingly, naïve CD8 T cells are able to rapidly, though transiently, produce IFN $\gamma$  following TCR triggering (8) and TLR2/7 signals (9). This early IFN $\gamma$  production by CD8 T cells has been suggested to mediate innate protection against *Listeria monocytogenes* (LM) (10), although others suggest that such IFN $\gamma$  derived from CD8 T cells may have a regulatory role rather than a direct innate function (9). Given the fact that IFN $\gamma$  is a key factor modulating the differentiation of CD4 T cells (11), it has been suggested that IFN $\gamma$  might also modulate CD8 T cell differentiation.

The balanced differentiation of CD8 T cells in effector and long-term memory subsets is crucial for immunity against intracellular pathogens. Variations in CD8 T cell fate have been extensively described based on their transcriptional profile, phenotype, function, and final anatomical location (12-14). But the underlying dynamic interactions that take place during early effector and memory CD8 T cell development are still poorly understood (15). The initial process of CD8 T cell activation is dependent on three signals (16): 1) antigenic stimulation; 2) engagement of costimulatory molecules; and 3) exposure to cytokines. These signals are largely provided by other cell types and integrated by the responding T cell, a well understood paradigm of CD8 T cell fate choice (17). However, several lines of evidence suggest that CD8 T cells can themselves tune their own fate. A T cell autonomous program of differentiation is initiated following brief antigenic stimulation and, in an antigen-independent manner, modulates the acquisition of effector and memory functions (18-20). In this context, T cell fate can then be influenced by stochastic levels of protein expression (21), autocrine or paracrine feedback loops (22-24), as well as direct T cell-T cell (T-T) co-regulation through soluble factors or synapse formation (25-29).

In this study, we took a top-down approach to study the direct involvement of IFN $\gamma$  in CD8 T cell differentiation in the context of LM infection. We determined that IFN $\gamma$  skews CD8 T cell generation towards memory generation during a specific temporal window. IFN $\gamma$ -dependent T cell fate occurs through a paracrine, “self-sufficient” mechanism, as CD8 T cells have a dominant sensitivity to their own IFN $\gamma$ , the first wave of which they produce within hours following antigen exposure. Inhibition of effector generation by IFN $\gamma$  involves accelerated downregulation of the Interleukin-2 (IL-2) receptor chain CD25, a known requirement for CD8 T cell memory commitment (30). By using a combination of *in vivo* imaging and *in vitro* experiments, we determined that activated CD8 T cells rely on the integration between IFN $\gamma$ R and integrin signaling, locally within T-T synapses to increase their responsiveness to IFN $\gamma$  through Src kinase signaling from integrins. Our data highlight a new model by which the integrin rich environment of T-T synapses specifically provides context and differentiation cues to newly activated CD8 T cells through specification of the signaling response to local IFN $\gamma$ .

## Results and Discussion

### Regulation of CD8 T cell differentiation through early secretion of IFN $\gamma$ .

To investigate the direct involvement of IFN $\gamma$  in CD8 T cell differentiation, we analyzed the effect of IFN $\gamma$  receptor (IFN $\gamma$ R) deletion in ovalbumin (OVA)-specific CD8 T cells (OTI) on their expansion following LM expressing OVA (LMOVA) infection. We found that the number of IFN $\gamma$ R<sup>-/-</sup> OTI T cells at the peak of the effector response was 20 times higher than their WT counterpart (**Fig.1A**), showing that direct IFN $\gamma$  signaling restricts CD8 T cell expansion. Because CD8 T cell differentiation is a dynamic process but knocking-out the allele is constitutive, we temporally inhibited IFN $\gamma$  with blocking antibodies and scored OTI frequency. An augmentation of OTI numbers was observed when IFN $\gamma$  was blocked 24 hours post-infection, but not later (**Fig.1B, S1A-B**). Similar increase in antigen-specific CD8 T cells following IFN $\gamma$  block at 24h was found when the endogenous response was assessed (**Fig.1C**), showing that this was not an artifact induced by transfer of transgenic T cells. This critical 24-hour window corresponds to a first wave of IFN $\gamma$  production following LM infection (**Fig.S1C**). Tracking OTI T cells over time revealed that blockade of this first wave of IFN $\gamma$  not only increased expansion specifically during the effector stage, but also restricted memory generation (**Fig.1D-E**). Memory cells generated when early IFN $\gamma$  was blocked were able to expand normally upon re-challenge with LMOVA (**Fig.1F**), but they displayed decreased IFN $\gamma$  and Granzyme B production (**Fig.1G-H**). Altogether, we concluded that IFN $\gamma$  produced around 24 hours after LM infection skews CD8 T cell differentiation towards memory.

The fact that early (24-48h) blocking of IFN $\gamma$  increased CD8 T cell numbers starting at day 7 (**Fig.1D**) suggested an indirect function of IFN $\gamma$  on cell expansion or contraction. Consistent with this, temporal IFN $\gamma$  blockade had no direct effect on OTI cell cycle, proliferation or apoptosis (**Fig.S1D-F**), nor did it affect expression of apoptosis or inhibitory receptors (**Fig.S1G-H**) during early effector expansion. These data suggested that IFN $\gamma$  regulated CD8 T cell effector differentiation per se as opposed to cell expansion. Surprisingly, IFN $\gamma$  did not modulate the ratio between the transcription factors t-bet and eomes (**Fig.S1I**), two master regulators of CD8 T cell differentiation. This suggested that IFN $\gamma$  impacted CD8 T cell differentiation through a non-canonical mechanism. IFN $\gamma$  can synergize or antagonize the effects of growth factors and cytokines (31). Because inflammatory cytokines favor effector differentiation by prolonging the expression of the Interleukin-2 receptor alpha chain CD25 (30, 32), we investigated the function of early IFN $\gamma$  secretion on CD25 expression. Regardless of IFN $\gamma$  blockade, virtually all primed OTI cells up-regulated CD25 2 days after infection, started to down-regulate CD25 after Day 4 and no longer expressed CD25 by Day 7 (**Fig.S1J**). However, IFN $\gamma$  blockade resulted in a higher percentage of OTI cells expressing CD25 during the down-regulation phase, with a higher MFI (**Fig.1I and S1J**). This resulted in enhanced IL-2 driven signaling in OTI T cells at this time, analyzed by Stat5 phosphorylation (**Fig.S1K**). Similar CD25 increase was found on endogenous CD8 T cells following IFN $\gamma$  blockade (**Fig.1J**). Prolonged CD25 expression at Day 5 is in agreement with increased effector and decreased memory formation detected from Day 7 and is consistent with IFN $\gamma$  antagonizing, or targeting the same pathway as inflammatory cytokines (33). Altogether, our data show that IFN $\gamma$  skews CD8 T cell differentiation towards memory formation by modulating CD25 expression.

### Spatio-temporal behavior of IFN $\gamma$ -producing cells during LM infection suggests a paracrine IFN $\gamma$ signaling in early activated CD8 T cells.

As IFN $\gamma$  delivered between 24h post-infection was sufficient to control CD8 T cell differentiation, we characterized the cell types producing IFN $\gamma$  *in situ* at this time. NK cell comprised 60% of IFN $\gamma$ -positive cells (**Fig.2A**). Additionally, activated CD8 T cells accounted for nearly 20% of the total IFN $\gamma$ -positive cells (**Fig.2A and Fig.S2A**), and IFN $\gamma$  production by CD8 T cells followed overall the same biphasic pattern (**Fig.2B**) seen for global IFN $\gamma$  production (**Fig.S1C**). Early IFN $\gamma$  production by CD8 T cells was not only a feature of memory cells as previously described (34) because activated cells coming from the naïve (CD44<sup>low</sup>) pool also contributed to IFN $\gamma$  production (**Fig.S2B**), albeit in lower quantity (**Fig.S2C**).

As IFN $\gamma$  derived from CD4 T cells is sufficient to mediate Th1 differentiation in the context of *Leishmania Major* infection (35), we hypothesized that CD8 T cell-derived IFN $\gamma$  might likewise be the dominant source regulating OTI differentiation. In support of this, genetic ablation of IFN $\gamma$  only in OTI T cells resulted in a greater number of effector T cells following LMOVA infection, almost to the same extent as seen for total antibody-mediated IFN $\gamma$  blockade (**Fig.2C**). Although endogenous CD8 T cells produced IFN $\gamma$ , they surprisingly did not fully compensate for the absence of IFN $\gamma$  in IFN $\gamma$ <sup>-/-</sup> OTI cells (**Fig.2C**). This was not due to an overproduction of IFN $\gamma$  by OTI cells compared to endogenous T cells, as OTI T cells represented approximately only 1/15<sup>th</sup> of all CD8 T cell IFN $\gamma$  producers (**Fig.S2D**). It therefore raised the question of whether IFN $\gamma$  signaling in T cells was autocrine or paracrine. To investigate this, we asked whether IFN $\gamma$  produced by WT OTI could induce signaling in IFN $\gamma$ <sup>-/-</sup> OTI cells, which would be indicative of paracrine signaling. *In vitro* co-culture (**Fig.2D**) and *in vivo* co-injection (**Fig.2E-F**) of IFN $\gamma$ <sup>-/-</sup> OTI cells with WT OTI T cells enhanced IFN $\gamma$  signaling in IFN $\gamma$ <sup>-/-</sup> OTI cells, assessed by Stat1 phosphorylation on Y701 24h after priming, suggesting paracrine IFN $\gamma$  signaling. Overall, CD8 T cells autonomously tune their differentiation, at least in part through early paracrine secretion of IFN $\gamma$  from other CD8 T cells.

How does this take place *in situ*? We hypothesized that a specific microenvironment providing other co-factors might be responsible for this alternate scenario. Twenty-four hours after LMOVA infection, IFN $\gamma$ -producing CD8 T cells were located in the white pulp, where they co-localize with other IFN $\gamma$ -producing cells such as NK cells that invaded the white pulp (**Fig.3A-B and Fig.S3A-B**), indicating that CD8 sensitivity to their own IFN $\gamma$  was not due to a segregation between CD8 T cells and other IFN $\gamma$ -producing cells. Assessment of cytokine distribution at the subcellular level *in situ* revealed that IFN $\gamma$  was vesicular and typically directed towards the interface with other cells in OTI cells while NK cells exhibited a more ubiquitous cellular localization pattern (**Fig.3C-D, Fig.S3C and Movie S1-2**). We previously described that T-T interactions occur after priming in the context of vaccination (26), interactions which would be in agreement with the directional IFN $\gamma$  secretion observed specifically between OTI T cells. Indeed, 2-photon microscopy revealed that T-T contacts occurred following LMOVA infection (**Movie S3**) with a dwell time of interaction of 10 minutes, while NK cells display shorter contacts with T cells (**Fig.3E-F**). For example, this resulted in 54.5% of OTI-OTI contacts and 18% of OTI-NK contacts when we scored contacts that lasted more than 5 minutes (**Fig.3G**). Using the mouse reporter Nur77-GFP coupled with CD8 *in situ* staining, we detected and tracked clusters of activated endogenous CD8 T cells 24h after LMOVA infection (**Fig.3H and Movie S4**), showing that clustering events were not due to the high precursor frequency of OTI cells transferred. We however noted that OTI clusters rarely contained endogenous activated CD8 T cells (**Fig.S3D**), which might be due to antigen-specificity and/or the rapid attraction towards chemokine niches in which the higher-affinity OTI might dominate over the mixed-affinity endogenous response. This would be consistent with the fact that expression of some chemokine receptors such as CXCR3 are regulated by T cell affinity (36). Importantly, clusters of endogenous CD8 T cells also mostly excluded NK cells as seen for OTI clusters (**Fig.S3E**). To conclude, CD8 T cells favored interactions with other CD8 T cells over NK cells *in vivo*, which could explain the dominance of paracrine IFN $\gamma$  signaling and its alternate outcome in early activated CD8 T cells.

#### Cell contacts are required to maximize IFN $\gamma$ signaling in activated CD8 T cells.

Our findings suggest that T-T contacts dictated the responsiveness of activated CD8 T cells to the IFN $\gamma$  they produce. These contacts rely on LFA-1 and ICAM-1 (26, 27, 37), and require LFA-1 activation downstream of T cell priming (38). We tested the effect of blocking these engagements with LFA-1 blocking antibodies in cultures where T cells were activated in a system devoid of APC. Inhibiting T-T contacts *in vitro* resulted in decreased Stat1 tyrosine phosphorylation (p(Y701)Stat1) downstream of IFN $\gamma$  (**Fig.4A and Fig.S4A**). This was not due to an inability of cells to produce or detect IFN $\gamma$  per se, since phosphorylation of Stat1 at another site, Serine 727, was unaffected (**Fig.4B and Fig.S4B**). Contact requirement for optimum IFN $\gamma$  signaling was not the consequence of a desensitization mechanism due to chronic IFN $\gamma$  exposure, as contacts were also required for increasing both the

amplitude and the sensitivity (as defined by EC50: Control=  $0.5 \pm 0.21$ ; LFA-1 Ab=  $4.3 \pm 0.19$ ) of IFN $\gamma$  signaling following acute exposure (**Fig.4C**). Requirement of contact for maximum IFN $\gamma$  signaling was also not the result of IFN $\gamma$ R downregulation (**Fig.S4C**), as observed for CD4 T cells differentiating into the Th1 subset (39). We thus concluded that cell-cell interactions potentiated the responsiveness of activated CD8 T cells to IFN $\gamma$ .

LFA-1 promotes cellular adherence and signaling in response to ligation (40), which could both potentially maximize IFN $\gamma$  signaling. We first addressed whether adherence and proximity were responsible for enhanced IFN $\gamma$  signaling by forcing OTI T cells treated with LFA-1 blocking antibody ("LFA-1less") to cluster in an integrin-independent manner by using a DNA zippering method, modified from (41, 42) (**Fig.4D**). Although this method allowed LFA-1less T cells to cluster to the same extent as control T cells (**Fig.S4D**), it did not lead to increased sensitivity (EC50: LFA-1 Ab=  $0.52 \pm 0.17$ ; LFA-1 Ab+oligos=  $0.32 \pm 0.18$ ) or amplitude of p(Y701)Stat1 (**Fig.4E**). Conversely, addition of plate-bound coated integrin was able to rescue IFN $\gamma$ -induced p(Y701)Stat1 of LFA-1less OTI T cells (**Fig.4F**) (EC50: LFA-1 Ab=  $4.1 \pm 0.17$ ; LFA-1 Ab+FN=  $0.36 \pm 0.22$ ), suggesting that integrin engagement was sufficient to potentiate of IFN $\gamma$  signaling in activated CD8 T cells. To further assess the sufficiency of integrins to mediate this effect, we used a system of beads where IFN $\gamma$  and integrins were co-delivered or delivered independently. Co-delivery was required for maximum amplitude of p(Y701)Stat1 generation (**Fig.4G**), suggesting that integrins had to co-localize with IFN $\gamma$ R to enable signal integration, consistent with IFN $\gamma$ R and ICAM-1 co-localization at T-T contacts (**Fig.4H-I**).

Altogether, we concluded that activated CD8 T cells responded to polarized engagement of integrin ligands and IFN $\gamma$  in a manner that co-stimulated IFN $\gamma$  signaling. We believe the term 'costimulation' is warranted in this situation since LFA-1 engagement on its own had little effect on Stat1 phosphorylation.

#### Integrin-mediated activation of Src Kinases enhances IFN $\gamma$ responsiveness of activated CD8 T cells and restricts effector differentiation.

To understand how integrin engagement potentiated IFN $\gamma$  signaling, we tested the function of the canonical integrin signaling intermediate Src kinases (Fyn or Lck in T cells) in potentiating IFN $\gamma$  signaling. We inhibited Src kinases using the inhibitor PP2 and compared this to inhibiting the JAK1/2 pathway using the selective inhibitor Ruxolitinib. While IFN $\gamma$  signaling in naïve OTI T cells, which cannot make T-T contacts, was inhibited by Jak but not Src inhibitors (**Fig.5A**), maximum p(Y701)Stat1 in activated OTI T cells was blocked by inhibitors of both pathways (**Fig.5B**). Src kinase inhibitor treatment did not result in decreased cell clustering (**Fig.S5A**). Consistent with integrin and IFN $\gamma$  signal integration, p(Y701)Stat1 was located at the T-T contact interface, and co-localized with the Src kinase Fyn (**Fig.5C-D**).

Because integrin signaling was necessary to potentiate IFN $\gamma$  signaling in activated OTI T cells, we hypothesized that inhibiting Src kinases specifically during the first wave of IFN $\gamma$  would mimic the effect of IFN $\gamma$  temporal blockade on CD8 T cell differentiation (**Fig.1B**). Similar to IFN $\gamma$  blockade, injection of Src kinase inhibitor 24 hours after LMOVA infection (**Fig.5E**) resulted in nearly a doubling of the number of effector OTI T cells (**Fig.5F**) and an increase in the effector to memory ratio (**Fig.5G**). Src inhibition did not affect apoptosis (**Fig.5H**) but resulted in prolonged CD25 expression (**Fig.5I**), phenocopying early IFN $\gamma$  block. The same effect on expansion (**Fig.S5B**) and CD25 expression (**Fig.S5C**) could be observed at the endogenous level. Finally, as Src kinases are also downstream of other events relevant to CD8 T cell activation, i.e TCR triggering, we also controlled that the effect of the Src inhibitor on OTI effector expansion we detected *in vivo* was not due to an interference with TCR triggering. To do so, we interrogated whether TCR component CD3 was clustered at T-T interface, which would be indicative of signaling. We did not find any evidence of CD3 localization at T-T synapses *in vitro* (**Fig.S5D**) and *in vivo* (**Fig.S5E**). We then blocked TCR triggering using a blocking antibody against MHC Class1 *in vivo*. Blocking MHC Class1 resulted in reduced OTI cell expansion when injected at the beginning of the infection as expected, and the same result was observed when blockade happened during clustering events (**Fig.S5F**). While this data does not necessarily negate a possible

involvement of TCR signaling at T-T contacts, it suggests that this is not the main pathway affected by Src inhibition at this time. Overall, this data support the requirement of integrin signaling during a specific time-window to restrict the CD8 T cell commitment to effector.

## Discussion

To conclude, we provide evidence of a new context dependent IFN $\gamma$  signaling resulting in the control of the balance between effector and memory CD8 T cell differentiation. We demonstrated that early IFN $\gamma$  production by CD8 T cells acts in a paracrine manner to limit effector CD8 T cell differentiation, and relies on co-engagement with integrins. The costimulation of IFN $\gamma$  by integrins at T-T synapses results in enhanced Stat1 phosphorylation, and is required *in vivo* for controlling CD8 T cell fate.

Altogether, our data argue that co-engagement of IFN $\gamma$ R and integrins at T-T synapses results in enhanced IFN $\gamma$  signaling. Although we do not know whether additional factors are required for signal integration, the fact that IFN $\gamma$ R must be recruited to lipid nanodomains to illicit signaling (43) raises the possibility that in activated CD8 T cells, integrins recruit IFN $\gamma$ R to specific lipid nanodomains at T-T synapses, enabling distinct downstream events. Consistent with this, we noted that conditions that could restrict plasma membrane “fluidity”, such as coating IFN $\gamma$  on beads or inserting lipid-DNA oligos in the plasma membrane, resulted in an inhibition of integrin-mediated sensitivity to IFN $\gamma$ , as analyzed by EC50, but did not have major effect on the increased amplitude of IFN $\gamma$  signaling. We speculate that this reflects the fact that reorganization of proteins at the plasma membrane is important for integrin-enhanced sensitivity to IFN $\gamma$ . Alternately, this could also reflect a requirement of endocytosis of the IFN $\gamma$ R/IFN $\gamma$  complex.

How IFN $\gamma$  regulates CD25 down-regulation is unclear. The fact that we observe a lag of 4 days between IFN $\gamma$  secretion and CD25 down-regulation suggests that IFN $\gamma$  does not directly regulates CD25 expression. Alternately, it has recently been shown that transient IFN $\gamma$  exposure elicits long-lived inflammatory responses in cancer cells due to IFN $\gamma$  retention by phosphatidylserine (PS) on the surface of viable cells (44). As TCR activation induces PS exposure at the surface of T cells (45), a similar mechanism could lead to long-term exposure of T cells to IFN $\gamma$ .

IFN $\gamma$  is typically associated with pro-inflammatory processes, but it also has regulatory properties (46). Our data provides another example where IFN $\gamma$  can be considered as regulating inflammation, as it counteracts prolonged CD25 expression known to be potentiated by inflammatory cytokines (30, 32). The balance between pro- and anti-inflammatory properties of IFN $\gamma$  could explain discrepancies between models, where IFN $\gamma$  limits effector expansion in some models (our study) (47, 48), but not all (24, 49). Our data demonstrating that integrin costimulation is required for limiting T cell effector generation suggest that the presence of co-factors represents one of a series of possible modifiers of IFN $\gamma$  signaling and function specification.

We also demonstrated that early IFN $\gamma$  production by CD8 T cells acts in a paracrine manner to limit effector CD8 T cell differentiation through integrin-mediated T-T contacts. But it is important to note that blocking IFN $\gamma$  (this study) does not phenocopy blocking T-T contacts as a whole (26). Whereas integration of IFN $\gamma$  and integrin signaling pathways restricts T cell effector differentiation, T-T contacts promote both effector and central memory differentiation (26). This discrepancy is likely due to the role T-T synapses play a ‘platform’, fostering a network of diverse signals shared exclusively between T cells. Some of these may also be temporal and include contributions from other cell-cell contacts *in vivo*. Our study provides one instance of such a platform function. Importantly, where integrin activation is dictated by the encounter with the antigen early during priming and will reflect strength of activation, IFN $\gamma$  secretion is determined by cell location and environment. Together, a platform of T-T synapses allows for those distinct signals to integrate themselves through costimulation of IFN $\gamma$  signaling by integrin co-engagement.

Although it is usually accepted that cytokine signals are tightly localized, affecting only cells near the cytokine source, cytokines can permeate a tissue and modify the majority of cells therein (50).

The polarized secretion of IFN $\gamma$  in CD8 T cells argues for localized cytokine delivery, but our data are not in contradiction with the existence of IFN $\gamma$  permeation, as NK cells do not seem to secrete IFN $\gamma$  in a polarized manner. Overall, this might imply that NK cells would be the source of systemic IFN $\gamma$  (51), whereas low levels of IFN $\gamma$  produced by CD8 T cells would be specifically directed towards its target with signaling amplified or specified further by integrin co-engagement. The fact that previous T cell activation is necessary for this (26) means that while IFN $\gamma$  might be spread throughout the spleen, only cells in the correct state of activation and engaging integrins will adequately respond to this cue. Overall, having methods to locally boost IFN $\gamma$  signaling by integrins at a synapse may optimize efficient T cell-mediated pathogen clearance programs while restricting harmful bystander responses.



## **Materials and Methods.**

### Cell isolation, activation and in vitro treatment.

OTI T cells were isolated from lymph nodes of 6- to 12-week-old mice. Selection was carried out with a negative CD8 isolation kit (Stemcell Technologies). For in vitro experiments, cells were activated in vitro at low density with PMA (2ng/ml) and Ionomycin (20ng/ml) and treated where indicated, with 10µg/ml anti-LFA-1 (M17.4; BioXCell), 10µM Src inhibitor PP2 (Sigma), 1µM Jak inhibitor Ruxolitinib (Santa Cruz biotechnology) for 3-6 h at 37C 5%CO<sub>2</sub>. Then cells were treated with the indicated dose of IFN-γ (Peprotech) for 20 min at 37C 5%CO<sub>2</sub>. In some experiments, cells were plated on Fibronectin (EMD Millipore)-coated plates.

### Infection and treatments.

OTI cells (5x10<sup>3</sup> cells for effector/memory assessment; 5 x10<sup>4</sup> for phenotyping at Day 5; 5 x10<sup>5</sup> for Hoechst and proliferation experiments), isolated as described above, were transferred into recipient C57Bl6 mice by retro-orbital or intravenous injection. Mice were infected 16 h later. Mice were given intravenous injection of 10<sup>3</sup> colony-forming units of *L. monocytogenes* expressing a secreted form of OVA (LMOVA) (52).

In some experiments, mice received one or two injections (separated by 12h, and centered around the indicated time point) of 75µg intra-peritoneal injection of isotype-matched control antibody (rat IgG1; BioXCell), anti- IFNγ (XMG1.2; BioXCell) or one single injection of 125-250µg Src inhibitor PP2 24h after infection, or one single injection of 250µg anti-MHC Class1 (AF6-88.5.5.3; BioXCell) at 0 or 24h after infection.

For recall experiments, mice were re-challenged 50 to 60 days after the primary infection with intravenous injection of 10<sup>3</sup> colony-forming units of LMOVA and analyzed after 5 days.

## **Acknowledgements**

We thank the Kennedy Institute Imaging Facility and the Biological Imaging Development Center personnel for technical assistance with imaging, and the NIH tetramer facility for the SIINFEKL tetramer. We thank E. Roberts, M. Headley, J. Bezbradica-Mirkovic and E. Thompson for critical reading of the manuscript. Ju.M is a student of the Master of Oncology of Lyon, France and was supported by the LabEx DEVweCAN, Université de Lyon, F-69000 Lyon, France. This work was supported by grants from NIH (R01AI052116 and R01AI114787 to M.F.K.; R03AI119220 to A.G.), from the Kennedy Trust (to A.G.) and BBSRC (BB/R015651/1 to A.G.).

## References

- Ikeda H, Old LJ, & Schreiber RD (2002) The roles of IFN gamma in protection against tumor development and cancer immunoediting. *Cytokine Growth Factor Rev* 13(2):95-109.
- Billiau A & Matthys P (2009) Interferon-gamma: a historical perspective. *Cytokine Growth Factor Rev* 20(2):97-113.
- Lees JR (2015) Interferon gamma in autoimmunity: A complicated player on a complex stage. *Cytokine* 74(1):18-26.
- Schroder K, Hertzog PJ, Ravasi T, & Hume DA (2004) Interferon-gamma: an overview of signals, mechanisms and functions. *Journal of leukocyte biology* 75(2):163-189.
- Bach EA, Aguet M, & Schreiber RD (1997) The IFN gamma receptor: a paradigm for cytokine receptor signaling. *Annual review of immunology* 15:563-591.
- Murray PJ (2007) The JAK-STAT signaling pathway: input and output integration. *J Immunol* 178(5):2623-2629.
- Ishihara K & Hirano T (2002) Molecular basis of the cell specificity of cytokine action. *Biochimica et biophysica acta* 1592(3):281-296.
- Hosking MP, Flynn CT, & Whitton JL (2014) Antigen-specific naive CD8+ T cells produce a single pulse of IFN-gamma in vivo within hours of infection, but without antiviral effect. *J Immunol* 193(4):1873-1885.
- Salerno F, Guislain A, Cansever D, & Wolkers MC (2016) TLR-Mediated Innate Production of IFN-gamma by CD8+ T Cells Is Independent of Glycolysis. *J Immunol* 196(9):3695-3705.
- Berg RE, Crossley E, Murray S, & Forman J (2005) Relative contributions of NK and CD8 T cells to IFN-gamma mediated innate immune protection against *Listeria monocytogenes*. *J Immunol* 175(3):1751-1757.
- Bradley LM, Dalton DK, & Croft M (1996) A direct role for IFN-gamma in regulation of Th1 cell development. *J Immunol* 157(4):1350-1358.
- Buchholz VR, Graf P, & Busch DH (2013) The smallest unit: effector and memory CD8(+) T cell differentiation on the single cell level. *Frontiers in immunology* 4:31.
- Kaech SM & Cui W (2012) Transcriptional control of effector and memory CD8+ T cell differentiation. *Nature reviews. Immunology* 12(11):749-761.
- Joshi NS & Kaech SM (2008) Effector CD8 T cell development: a balancing act between memory cell potential and terminal differentiation. *J Immunol* 180(3):1309-1315.
- Krummel MF, Bartumeus F, & Gerard A (2016) T cell migration, search strategies and mechanisms. *Nature reviews. Immunology* 16(3):193-201.
- Pennock ND, et al. (2013) T cell responses: naive to memory and everything in between. *Adv Physiol Educ* 37(4):273-283.
- Obar JJ & Lefrancois L (2010) Early events governing memory CD8+ T-cell differentiation. *International immunology* 22(8):619-625.
- van Stipdonk MJ, Lemmens EE, & Schoenberger SP (2001) Naive CTLs require a single brief period of antigenic stimulation for clonal expansion and differentiation. *Nature immunology* 2(5):423-429.
- Kaech SM & Ahmed R (2001) Memory CD8+ T cell differentiation: initial antigen encounter triggers a developmental program in naive cells. *Nature immunology* 2(5):415-422.
- Mercado R, et al. (2000) Early programming of T cell populations responding to bacterial infection. *J Immunol* 165(12):6833-6839.
- Feinerman O, Veiga J, Dorfman JR, Germain RN, & Altan-Bonnet G (2008) Variability and robustness in T cell activation from regulated heterogeneity in protein levels. *Science* 321(5892):1081-1084.
- Long M & Adler AJ (2006) Cutting edge: Paracrine, but not autocrine, IL-2 signaling is sustained during early antiviral CD4 T cell response. *J Immunol* 177(7):4257-4261.
- O'Brien S, et al. (2014) Ikaros imposes a barrier to CD8+ T cell differentiation by restricting autocrine IL-2 production. *J Immunol* 192(11):5118-5129.
- Curtsinger JM, Agarwal P, Lins DC, & Mescher MF (2012) Autocrine IFN-gamma promotes naive CD8 T cell differentiation and synergizes with IFN-alpha to stimulate strong function. *J Immunol* 189(2):659-668.
- Thaventhiran JE, et al. (2012) Activation of the Hippo pathway by CTLA-4 regulates the expression of Blimp-1 in the CD8+ T cell. *Proceedings of the National Academy of Sciences of the United States of America* 109(33):E2223-2229.
- Gerard A, et al. (2013) Secondary T cell-T cell synaptic interactions drive the differentiation of protective CD8+ T cells. *Nature immunology* 14(4):356-363.

27. Zumwalde NA, Domaie E, Mescher MF, & Shimizu Y (2013) ICAM-1-dependent homotypic aggregates regulate CD8 T cell effector function and differentiation during T cell activation. *J Immunol* 191(7):3681-3693.
28. Klebanoff CA, *et al.* (2016) Memory T cell-driven differentiation of naive cells impairs adoptive immunotherapy. *The Journal of clinical investigation* 126(1):318-334.
29. Polonsky M, *et al.* (2018) Induction of CD4 T cell memory by local cellular collectivity. *Science* 360(6394).
30. Kalia V, *et al.* (2010) Prolonged interleukin-2Ralpha expression on virus-specific CD8+ T cells favors terminal-effector differentiation in vivo. *Immunity* 32(1):91-103.
31. Hu X & Ivashkiv LB (2009) Cross-regulation of signaling pathways by interferon-gamma: implications for immune responses and autoimmune diseases. *Immunity* 31(4):539-550.
32. Pipkin ME, *et al.* (2010) Interleukin-2 and inflammation induce distinct transcriptional programs that promote the differentiation of effector cytolytic T cells. *Immunity* 32(1):79-90.
33. Belz GT & Masson F (2010) Interleukin-2 tickles T cell memory. *Immunity* 32(1):7-9.
34. Kambayashi T, Assarsson E, Lukacher AE, Ljunggren HG, & Jensen PE (2003) Memory CD8+ T cells provide an early source of IFN-gamma. *J Immunol* 170(5):2399-2408.
35. Wakil AE, Wang ZE, Ryan JC, Fowell DJ, & Locksley RM (1998) Interferon gamma derived from CD4(+) T cells is sufficient to mediate T helper cell type 1 development. *The Journal of experimental medicine* 188(9):1651-1656.
36. Ozga AJ, *et al.* (2016) pMHC affinity controls duration of CD8+ T cell-DC interactions and imprints timing of effector differentiation versus expansion. *The Journal of experimental medicine* 213(12):2811-2829.
37. Sabatos CA, *et al.* (2008) A synaptic basis for paracrine interleukin-2 signaling during homotypic T cell interaction. *Immunity* 29(2):238-248.
38. Dustin ML & Springer TA (1989) T-cell receptor cross-linking transiently stimulates adhesiveness through LFA-1. *Nature* 341(6243):619-624.
39. Bach EA, *et al.* (1995) Ligand-induced autoregulation of IFN-gamma receptor beta chain expression in T helper cell subsets. *Science* 270(5239):1215-1218.
40. Hogg N, Patzak I, & Willenbrock F (2011) The insider's guide to leukocyte integrin signalling and function. *Nature reviews. Immunology* 11(6):416-426.
41. Weber RJ, Liang SI, Selden NS, Desai TA, & Gartner ZJ (2014) Efficient targeting of fatty-acid modified oligonucleotides to live cell membranes through stepwise assembly. *Biomacromolecules* 15(12):4621-4626.
42. Taylor MJ, Husain K, Gartner ZJ, Mayor S, & Vale RD (2017) A DNA-Based T Cell Receptor Reveals a Role for Receptor Clustering in Ligand Discrimination. *Cell* 169(1):108-119 e120.
43. Blouin CM, *et al.* (2016) Glycosylation-Dependent IFN-gammaR Partitioning in Lipid and Actin Nanodomains Is Critical for JAK Activation. *Cell* 166(4):920-934.
44. Oyler-Yaniv A, *et al.* (2017) A Tunable Diffusion-Consumption Mechanism of Cytokine Propagation Enables Plasticity in Cell-to-Cell Communication in the Immune System. *Immunity* 46(4):609-620.
45. Fischer K, *et al.* (2006) Antigen recognition induces phosphatidylserine exposure on the cell surface of human CD8+ T cells. *Blood* 108(13):4094-4101.
46. Muhl H & Pfeilschifter J (2003) Anti-inflammatory properties of pro-inflammatory interferon-gamma. *Int Immunopharmacol* 3(9):1247-1255.
47. Badovinac VP, Tvinnereim AR, & Harty JT (2000) Regulation of antigen-specific CD8+ T cell homeostasis by perforin and interferon-gamma. *Science* 290(5495):1354-1358.
48. Sercan O, Stoycheva D, Hammerling GJ, Arnold B, & Schuler T (2010) IFN-gamma receptor signaling regulates memory CD8+ T cell differentiation. *J Immunol* 184(6):2855-2862.
49. Whitmire JK, Tan JT, & Whitton JL (2005) Interferon-gamma acts directly on CD8+ T cells to increase their abundance during virus infection. *The Journal of experimental medicine* 201(7):1053-1059.
50. Perona-Wright G, Mohrs K, & Mohrs M (2010) Sustained signaling by canonical helper T cell cytokines throughout the reactive lymph node. *Nature immunology* 11(6):520-526.
51. Kim D, Reilly A, & Lawrence DA (2001) Relationships between IFNgamma, IL-6, corticosterone, and Listeria monocytogenes pathogenesis in BALB/c mice. *Cellular immunology* 207(1):13-18.
52. Pope C, *et al.* (2001) Organ-specific regulation of the CD8 T cell response to Listeria monocytogenes infection. *J Immunol* 166(5):3402-3409.

## Figure Legends

### Figure 1: Regulation of CD8 T cell differentiation through early secretion of IFN $\gamma$ .

**A-** Mice bearing WT and IFN $\gamma$ R<sup>-/-</sup> OTI cells (ratio 1:1) were infected with LMOVA. Graph shows the number of effector WT or IFN $\gamma$ R<sup>-/-</sup> OTI analyzed by flow cytometry at Day 10. Data are from two independent experiments, n=4. **(B-I)** WT Mice **(C)** bearing OTI **(B,D-I)** were infected with LMOVA. When indicated, mice were treated with blocking IFN $\gamma$  24h post-infection (Ab), or otherwise stated. **B-** The phenotype of OTI in the spleen was analyzed when by flow cytometry. Graph shows the percentage of OTI among CD8 T cells 10 days post-infection. Data are from three independent experiments, n=5. **C-** Frequency of OVA-specific cells among endogenous CD8 T cells was analyzed 8 days after infection by flow cytometry. Data are from three independent experiments, n=15. **D-** Graph shows the number of OTI over time. Data are from two independent experiments, n=6. **E-** Graph shows the number of memory (KLRG1<sup>-</sup> CD127<sup>+</sup>) OTI 45 days post infection. Data are from two independent experiments, n=6. **(F-H)** Mice were re-challenged with LMOVA 50 to 60 days post-primary challenge and analyzed after 5 days. Data are from three independent experiments, n=12. **F-** Graph shows the number of OTI quantified by flow cytometry. **(G-H)** Splenocytes were re-stimulated in vitro with PMA and Ionomycin in the presence of Brefeldin A. Graphs show the percentage of OTI expressing IFN $\gamma$  (G) and Granzyme B (H). **I-** Histograms show CD25 expression on OTI 5 days post- primary infection. Data are from three independent experiments, n=7. **J-** Frequency of CD25 positive endogenous total CD8 T was analyzed by flow cytometry 5 days after infection with LMOVA in the presence or absence of IFN $\gamma$  Ab blockade at 24h (Ab). Data are from three independent experiments, n=6.

### Figure 2: Autonomous regulation of CD8 T cell differentiation through paracrine IFN $\gamma$ signaling.

**(A-B)** Mice were infected with LM-OVA and treated with BFA 6 hours before being sacrificed. **A-** The different cell populations among IFN $\gamma$  positive splenocytes 24 hours after infection were analyzed by flow cytometry. Splenocytes were first gated on IFN $\gamma$  positive cells, and the different populations within the IFN $\gamma$  positive cells were defined using the antibodies NK1.1, CD8, CD4, CD19, and  $\gamma\delta$ TCR. **B-** The percentage of CD8 T cells producing IFN $\gamma$  was analyzed by flow cytometry over time. Data are from at least 3 independent experiments, n=6-8. **C-** Mice bearing WT or IFN $\gamma$ R<sup>-/-</sup> OTI were infected with LM-OVA. When indicated, mice were treated with blocking IFN $\gamma$  Ab 24 hours post infection (Ab). Graph shows the number of effector (KLRG1<sup>+</sup> CD127<sup>-</sup>) OTI per 1/3 spleen. Data are from two independent experiments, n=5. **D-** WT or IFN $\gamma$ R<sup>-/-</sup> OTI were stimulated with PI for 24h, either separated or in co-culture, and analyzed by flow cytometry. Representative histograms showing Stat1 phosphorylation on tyrosine 701 (pStat1 (Y701)). Grey: WT OTI; Red: IFN $\gamma$ R<sup>-/-</sup> OTI; Blue: IFN $\gamma$ R<sup>-/-</sup> OTI when they are co-cultured with WT OTI. **(E-F)** Mice transferred with IFN $\gamma$ R<sup>-/-</sup> OTI with or without WT OTI (ratio 1.1), were infected with LM-OVA. After 24h, splenocytes were analysed by flow cytometry. **E-** Representative histogram showing pStat1 (Y701) staining in IFN $\gamma$ R<sup>-/-</sup> OTI. Red: IFN $\gamma$ R<sup>-/-</sup> OTI only; Blue: IFN $\gamma$ R<sup>-/-</sup> OTI co-cultured with WT OTI. **F-** Graph shows the percentage of pStat1 (Y701) positive IFN $\gamma$ R<sup>-/-</sup> OTI. Data are from two independent experiments, n=6.

### Figure 3: Dynamic localization of IFN $\gamma$ -secreting cells suggests a contact-dependent regulation of CD8 T cell differentiation.

**(A-D)** NCR1-GFP **(A-C)** or WT **(D)** mice were transferred with CMTMR-labelled OTI cells, infected with LM-OVA and sacrificed 24h after infection. Mice were treated with BFA 6h before harvest. **A-** Picture is a representative example of the localization of IFN $\gamma$  (blue)-producing OTI (red) relative to other IFN $\gamma$ <sup>+</sup> cells such as NK cells (green). Scale bars, 100  $\mu$ m. **B-** Quantification of the localization of IFN $\gamma$ -producing OTI relative to NK cells. Data are from four independent experiments. **(C-D)** Pictures are representative example of IFN $\gamma$ -producing NK and OTI at different scales: 10 **(C)**, 2  $\mu$ m (OTI) or 3  $\mu$ m (NK) **(D)**. Dotted lines delimit cell edges. **(E-G)** NCR1-GFP mice were transferred with 1x10<sup>6</sup> CMTMR-labelled OTI and infected with LM-OVA. After 24 hours, spleens were imaged by 2-photon microscopy for a period of 30 minutes at 30-second intervals. Data are from three independent experiments. **E-**

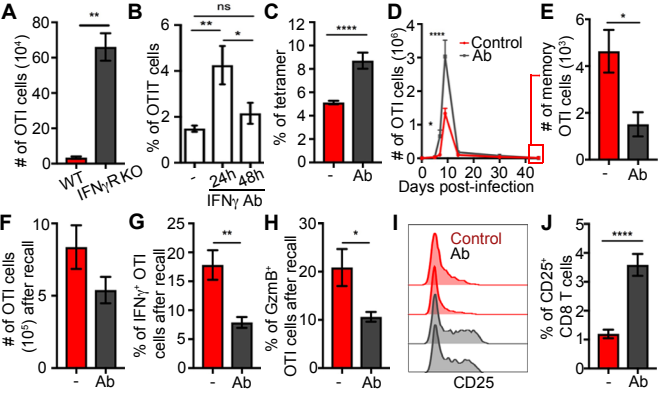
Snapshot of OTI- and NK-overlapping region. Tracks of OTI (red) and NK (green) cells over a 30-minute time-lapse are displayed. Scale bars, 10  $\mu$ m. **F**- Graph shows the percent of OTI remaining in contact with another OTI (red) or an NK cell (green) over time. **G**- Graph shows the percentage of OTI that are in contact for more than 5 minutes with another OTI (red) or a NK (green) cell. Each dot represents an individual field. **H**- Representative image of spleen section of Nur77-GFP mice 24h after infection with LM-OVA. Spleen sections were stained for GFP (white) and CD8 (purple). White edge delineates a cluster of activated CD8 T cells. Scale bars, 2  $\mu$ m.

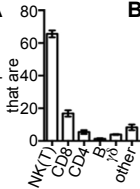
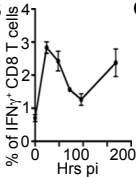
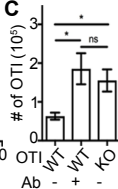
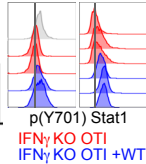
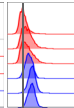
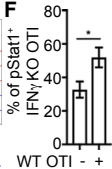
**Figure 4: Contact-dependent IFN $\gamma$  signaling in early activated CD8 T cells.**

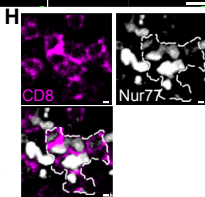
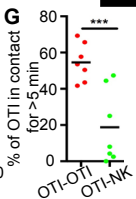
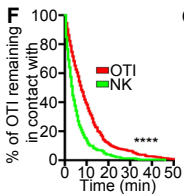
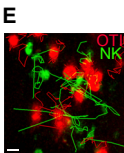
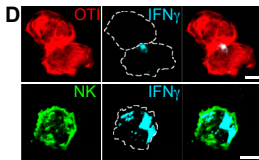
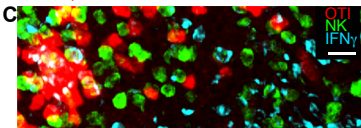
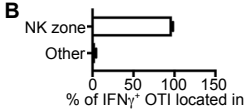
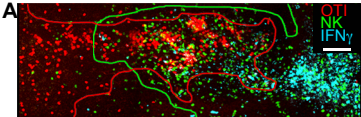
WT (**A, B, H**) or IFN $\gamma$ <sup>-/-</sup> (**A-C, E-G**) OTI were stimulated with PMA and Ionomycin for 24 hours. Where indicated, cells were treated with LFA-1 blocking Ab (LFA-1 Ab) or control Ab (RatIgG2a) 5 hours before harvest. (**A-B**) p(Y701) (**A**) and p(S727) (**B**) Stat1 was analyzed by western blot. Quantification (in bold) corresponds to the intensity ratio between phosphorylated and total Stat1. (**C-F**) The indicated amount of IFN $\gamma$  was added 20 minutes before harvest. Data are from three independent experiments. **C**- Graph shows p(Y701)Stat1 according to the dose of IFN $\gamma$ . (**D-E**) LFA-1 Ab-treated cells were forced to interact in an integrin-independent manner using fatty-acid modified oligonucleotides for 3 hours. **D**- Cartoon illustrating the strategy of oligonucleotide coating and forced proximity. Fatty acid-linked DNA oligos (blue) were inserted in the outer leaflet of the plasma membrane, and stabilized with DNA oligo anchors (orange). Oligo-labelled T cells were forced to stay aggregate by using complementary oligos (blue and red), leading to DNA hybridization. **E**- Graph shows p(Y701)Stat1 according to the dose of IFN $\gamma$ . Black line with circle= Mock-treated cells, Black line with triangles= LFA-1 Ab-treated cells, Gray line with squares= LFA-1 Ab-treated cells with oligonucleotides. n=6. **F**- When indicated, cells were plated on fibronectin (FN) for 2 hours before IFN $\gamma$  treatment. Graph shows p(Y701)Stat1 according to the dose of IFN $\gamma$ . Black line with circle= Mock-treated cells, Black line with triangles=LFA-1 Ab-treated cells, Gray line with squares= LFA-1 Ab-treated cells deposited on fibronectin coated-plates. n=6. **G**- Cells were incubated with IFN $\gamma$ -coated beads (Circle), IFN $\gamma$ -coated beads + FN-coated beads (Triangles), or IFN $\gamma$ /FN-co-coated beads (Squares) for 20 minutes. Graph shows p(Y701)Stat1 according to the quantity of IFN $\gamma$  coated on the beads. (**H-I**) 24h Activated OTI stained for ICAM-1 (green, left panel), IFN $\gamma$ R1 (red, middle panel) and the nucleus (dapi, blue in the merge right panel). **H**- Representative Image of T cell clusters. Scale bars, 4  $\mu$ m. **I**- Quantification of ICAM-1 and IFN $\gamma$ R1 co-localization at T-T contacts.

**Figure 5: Integrin signaling is required for optimum IFN $\gamma$  signaling in early activated CD8 T cells and for CD8 T cell differentiation in vivo.**

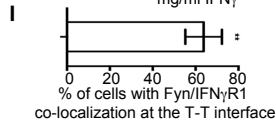
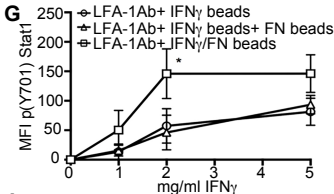
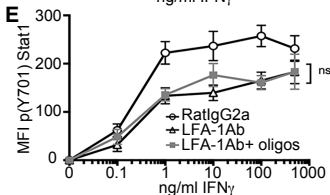
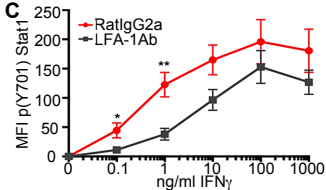
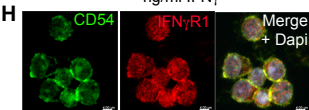
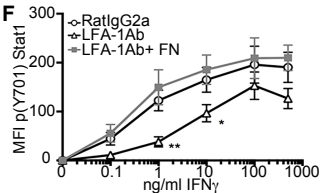
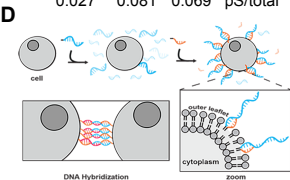
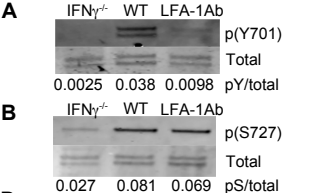
**A**- Naïve OTI were incubated with Src or Jak inhibitor (Inh) for 3 hours and treated for 20 minutes with IFN $\gamma$ . IFN $\gamma$  signaling was analyzed by p(Y701)Stat1 using flow cytometry. (**B-D**) OTI were stimulated at low density with PMA and Ionomycin for 24 hours. **B**- When indicated, cells were treated with LFA-1 blocking antibodies (LFA-1 Ab) from the time of activation, and src or jak inhibitor 5 hours before harvest. IFN $\gamma$  signaling was analyzed by p(Y701)Stat1 using flow cytometry. (**C-D**) 24h activated OTI were stained for Fyn (green, left panel), p(Y701)Stat1 (red, middle panel) and the nucleus (dapi, blue in the merge right panel). **C**- Representative Image of T cell clusters. **D**- Quantification of Fyn and p(Y701)Stat1 co-localization at T-T contacts. (**E-I**) Mice bearing OTI were infected with LM-OVA. When indicated, mice (n=10) were treated with src inhibitor 24 hours post-infection. The phenotype of OTI in the spleen was analyzed by flow cytometry using the antibodies CD8, CD45.1, KLRG1, CD127 and CD25. **E**- Cartoon illustrating the experimental setup. **F**- Graph shows the number of effector (KLRG1<sup>+</sup>CD127<sup>-</sup>) OTI per 1/3 spleen 10 days after infection. n=18. **G**- Graph shows the ratio between effector (KLRG1<sup>+</sup>CD127<sup>-</sup>) and precursor memory (KLRG1<sup>-</sup>CD127<sup>+</sup>) OTI T cells 10 days after infection. n=15 **H**- Graph shows the percentage of Annexin V<sup>+</sup> OTI 5 days after infection. **I**- Graph shows the percentage of CD25<sup>+</sup> OTI 5 days after infection. Data are from four (**A-D**), two (**F,H**) or three (**G,I**) independent experiments.

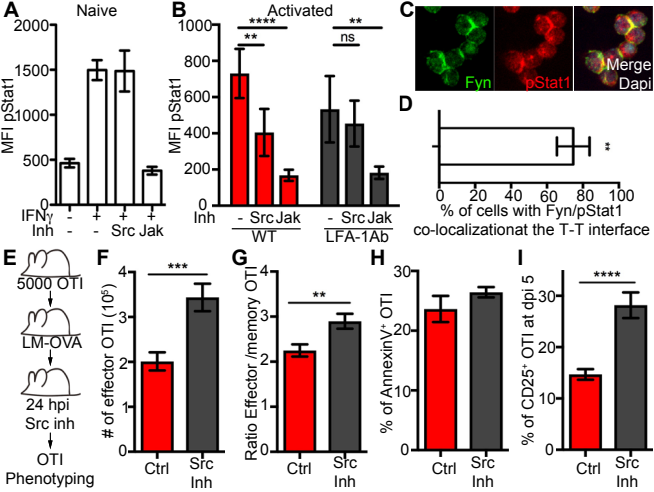


**A**% of IFN $\gamma$ <sup>+</sup> cells  
that are**B****C****D****E****F**











## Supplementary Information for

### **Paracrine Costimulation of IFN $\gamma$ Signaling by Integrins modulates CD8 T cell differentiation**

Matthew F. Krummel, Jagdish N. Mahale, Lion F.K. Uhl, Emily A. Hardison, Adriana M. Mujal, Julie M. Mazet, Robert J. Weber, Zev J. Gartner, and Audrey Gérard

\*Correspondence: [audrey.gerard@kennedy.ox.ac.uk](mailto:audrey.gerard@kennedy.ox.ac.uk) or [matthew.krummel@ucsf.edu](mailto:matthew.krummel@ucsf.edu)

#### **This PDF file includes:**

Supplementary text  
Figs. S1 to S5  
Captions for movies S1 to S4  
References for SI reference citations

#### **Other supplementary materials for this manuscript include the following:**

Movies S1 to S4

## Supplementary Text

### Supplementary Materials and Methods.

#### Mice.

IFN $\gamma$ <sup>-/-</sup> and IFN $\gamma$ R<sup>-/-</sup> mice (The Jackson Laboratory) were crossed with OTI mice to generate IFN $\gamma$ <sup>-/-</sup> OTI mice and IFN $\gamma$ R<sup>-/-</sup> OTI mice. Those mice, C57BL/6 mice (The Jackson Laboratory and Simonsen), and CD45.1<sup>+</sup>, OTI and NCR1-GFP mice (The Jackson Laboratory) were housed and bred under specific pathogen-free conditions at the University of California Animal Barrier Facility. All experiments involving mice were approved by the Institutional Animal Care and Use Committee of the University of California and in agreement with the UK Scientific Procedures Act of 1986.

#### Bead coating with IFN $\gamma$ and Fibronectin.

OTI cells were treated 16 hours after PMA and Ionomycin activation with beads (ratio 1.1) coated with different quantity of IFN $\gamma$  and or Fibronectin for 20 min. For beads coating, 6 $\mu$ m Microspheres (Polysciences) were incubated with the indicated amount of proteins OVN at 4C in Borate Buffer (PBS 50 mM Borate, pH 8.5), washed and saturated with PBS 2% BSA for 3 hours at RT. Beads were kept in PBS 1%BSA 5% glycerol at 4C. Bead coating was checked by flow cytometry.

#### Cell clustering using fatty-acid modified oligonucleotides.

*Fatty Acid-Modified Oligonucleotide Synthesis:* The methods for producing fatty acid-modified oligonucleotides and using them to label cells have been previously described in detail (1). Briefly, an Expedite 8909 DNA synthesizer using standard settings and reagents obtained from Glen Research was used to produce oligonucleotides linked to a solid support. Terminal amines were incorporated into completed oligonucleotides by a phosphoramidite or solid support for the adhesion and co-anchor strands respectively. The amines were used in a carbodiimide mediated condensation reaction with lignoceric and palmitic acids for the adhesion and co-anchor strands respectively. The solid support was washed with dichloromethane and dimethylformamide to remove excess reactants. The oligonucleotides were cleaved from the solid support and fatty-acid modified products were separated from unmodified oligonucleotides by reverse phase chromatography on an HPLC system. The product was lyophilized and the final concentration was determined by measure absorbance at 260 nm using a Thermo-Fischer Nanodrop system. In this study, 3 sequences were used, A, A', and Co-Anchor. Their sequences and fatty acid modifications are below.

A: 5'-C24-GTA ACG ATC CAG CTG TCA CT(T)<sub>60</sub> ACT GAC TGA CTG ACT GAC TG-3'

A': 5'-C24-GTA ACG ATC CAG CTG TCA CT(T)<sub>60</sub> CAG TCA GTC AGT CAG TCA GT-3'

Co-Anchor: 5' AGT GAC AGC TGG ATC GTT AC-C16-3'

*Cell Labeling:* Prior to labeling, cells were washed with calcium and magnesium-free phosphate-buffered saline (CMF PBS) to remove serum components that interfere with cell labeling. After washing, cells were resuspended in CMF PBS at a concentration of 1 million cells per 50  $\mu$ L and split equally into two tubes. Cells were labeled by incubation with 2  $\mu$ M of adhesion strand A in the first tube and A' in the second tube for 5 minutes on ice. This was followed by incubation with 2  $\mu$ M of co-anchor strand in both tubes for 5 minutes on ice. Cells were washed three times with phosphate-buffered saline to remove excess oligos.

*Cell Clustering:* Cells labeled with A and A' were mixed at a ratio of 1:20 in CMF PBS and pelleted to enforce aggregation by surface-labeled oligonucleotides. The pellet was gently resuspended with a 1 mL pipet to avoid disrupting aggregates. Aggregates were passed over a 70  $\mu$ m filter and aggregates that adhered to the filter were retained for experimentation.

#### Surface and intracellular flow cytometry staining.

For *in vivo* OTI T cell phenotyping, the spleen was excised at the indicated time after infection and a cell suspension was obtained. Cells were washed in PBS, and nonspecific binding was blocked with flow cytometry buffer (2% FCS, 2 mM EDTA and 0.02% sodium azide in PBS) containing anti-CD16/CD32 (2.4G2; UCSF Hybridoma Core). Surface proteins on cells were stained for 20 min at 4°C with the following fluorescence-conjugated antibodies in flow cytometry buffer: CD45.1 (A20), CD45.2 (104), CD8 (53.6.72), CD69 (H1.2F3), CD25 (3C7), CD95 (SA367H8), PD-1 (29F.1A12), KLRG1 and IL-7R (B12-1) (all from Biolegend). Cells were washed and resuspended in flow cytometry buffer containing 1% PFA.

For quantification of endogenous OVA-specific CD8 T cells, splenocytes were stained with Alexa647 conjugated to an MHC class I tetramer specific for SIINFEKL (National Institutes of Health Tetramer Core Facility (Emory University, Atlanta, GA)) in flow cytometry buffer. Subsequently, cells were stained for CD8 and analyzed by flow cytometry.

For staining of intracellular cytokines, mice were treated with an i.p. injection of 250 µg of brefeldinA (BFA, Sigma-Aldrich) 6 hours before being sacrificed at the indicated time after infection. Cells were stained for the following surface markers: NK1.1 (PK136), CD8 (53-6.7), CD4 (RM4-5), CD19 (6D5), and γδ TCR (GL3) (all from Biolegend) as described above, and fixed in flow cytometry buffer plus 2% PFA. Cells were then permeabilized for 5 min with flow cytometry buffer containing 2% saponin and were stained for 15 min at 20°C with fluorescence-conjugated anti-IFNγ (XMG1.2; eBiosciences) in flow cytometry buffer and 1% saponin. Cells were kept in flow cytometry buffer and 1% PFA before analysis.

For cell cycle assessment with Hoechst staining and proliferation, harvested splenocytes from mice bearing CFSE-labeled OTI cells were stained for CD8, CD45.1 and CD69, washed with PBS, fixed in 70% ethanol for 30 min on ice and washed twice with PBS. Cells were then incubated with PBS containing 0.1% Triton X-100, 0.1 mM EDTA, 100 µg/ml RNase A (Thermo Scientific), and 10 µg/ml Hoechst dye (Thermo Scientific). Cells were again washed and resuspended in flow cytometry buffer.

For *in situ* staining of intracellular cytokine signaling in OTI cells, cells were fixed with PBS 4% PFA. Cells were then incubated in ice-cold methanol and kept at -80°C OVN. Cells were extensively washed in FACS buffer and stained for 1h at 20°C with Alexa488-p(Y701)Stat1 (58D6; Cell Signaling), pS(727)Stat1 (Cell Signaling) followed by 1h with anti-Rabbit-Alexa488 or FITC-p(Y694)Stat5. Cells were kept in flow cytometry buffer before analysis.

For recall experiments, splenocytes were isolated 5 days after re-challenge and re-stimulated *in vitro* for 4 hours with PMA (50ng/ml; Sigma-Aldrich) and Ionomycin (500ng/ml; Sigma-Aldrich) in the presence of 5ug/ml Brefeldin A. Intra-cellular stainings with IFNγ and Granzyme B (QA16A02, Biolegend) antibodies were then performed as described above.

## **Western blot.**

Lysates from WT or IFNγ<sup>-/-</sup> OTI activated *in vitro* for 16-24h with PMA and Ionomycin were prepared in standard RIPA lysis buffer (150mM sodium chloride, 1.0% NP-40 or Triton X-100, 0.5% sodium deoxycholate, 0.1% SDS (sodium dodecyl sulfate), 50 mM Tris pH 8.0, protease inhibitor and PhosSTOP (Sigma)) for 10 min at 4°C and centrifuged at 13,000 rpm for 10 min at 4°C. Cell lysates were denatured with SDS, and separated by SDS-PAGE.

For immunoblotting, membranes were blocked and probed with specific pY(701)Stat1, pS(727)Stat1 and total Stat1 (all from Cell Signaling), and then incubated with the secondary antibodies (IRDye® 800CW anti-Rabbit and IRDye® 680LT anti-Mouse; LI-COR Biosciences). Immunoreactive bands were visualized with the Odyssey Imager and quantified with Image Studio.

## **Immunofluorescence and confocal microscopy.**

OTI cells were activated with 2ng/ml PMA and 20ng/ml ionomycin. After 24 h, cells were deposited on poly-L-Lysine-coated chambers for 30 min at 37°C, then fixed for 15 min at 4°C with 1% PFA. Cells were permeabilized in PBS 2% Saponin for 10 min at 20°C, and stained with the following antibodies: FITC-anti CD54 (YN1/1.7.4, ebiosciences), anti-IFN $\gamma$ R1 (C-20; Santa Cruz), anti-Fyn (E-3; Santa Cruz), anti-p(701)Stat1 (58D6; Cell Signaling) for 1h at 20°C. Cells were washed and stained with A488-anti mouse (for Fyn) and A568-anti rabbit (for fyn and p(701)Stat1) for 1h at 20°C. Cells were mounted on coverslips and analyzed with a Nikon A1R or an Olympus confocal microscope using a 25x/1.1 NA Plan Apo, water immersion objective or a 60x/1.2 NA Plan Apo, oil immersion objective. Imaris (Bitplane) and ImageJ were used for data analysis.

## **Histology.**

WT or Nur77-GFP mice were transferred with  $2 \times 10^6$  CMTMR-labeled OTI and infected with  $10^4$  cfu LM-OVA. Mice were treated with 250ug BFA when indicated 6 hours before sacrificed. After 16 to 24 h, mice were euthanized and spleens were removed and cryopreserved in OCT. Serial sections (30-40 $\mu$ m in thickness) of frozen spleens were stained with PB-B220, Alexa647-CD169, Alexa 488-GFP, Alexa594-CD8, BV421-IFN $\gamma$  or biotinylated-IFN $\gamma$  antibodies OVN at 4C in a humidified chamber. For biotinylated-IFN $\gamma$  staining, sections were then washed and incubated with DyLight 649-conjugated anti-rat (112-496-075; Jackson ImmunoResearch). All sections were analyzed by confocal microscopy.

NK- and OTI- rich region were manually identified without concurrent observation of the other cell distributions. Regions were labeled as NK-rich or OTI-rich if at least 8 NK or OTI cells, respectively, were present in 10 000  $\mu$ m<sup>2</sup>. Endogenous CD8 T cell clusters were defined as containing at least 8 CD8<sup>+</sup>Nur77-GFP<sup>+</sup> adjacent cells.

## **Two-photon imaging of explanted spleens.**

Nur77-GFP<sup>+/-</sup> and NCR1-GFP<sup>+/-</sup> mice were transferred with  $1 \times 10^6$  CMTMR-labeled OTI when indicated and infected with  $10^4$  cfu LM-OVA. Spleens were removed, sliced in 2 using a vibratome to expose the white pulp, and subsequently immobilized on coverslips with the white pulp facing up. For Nur77-GFP mice, spleen sections were stained for 15 minutes with 10  $\mu$ g/ml CD8-Alexa 594 before imaging.

Time-lapse imaging was performed with a custom-built 2-photon setup equipped with two infrared lasers (MaiTai, Spectra Physics; Chameleon, Coherent). The MaiTai laser was tuned to 810 nm for excitation of CMTMR. Chameleon laser excitation was tuned to 910 nm for excitation of GFP. Emitted light was detected using a 25 $\times$ 1.2NA water lens (Zeiss) coupled to a 6-colour detector array (custom; using Hamamatsu H9433MOD detectors). Emission filters used were: green 510/42, and red 607/70. The microscope was controlled by the MicroManager software suite. Images of up to 35 xy planes with 3- $\mu$ m z-spacing were acquired every 30 s for 30 min.

Imaris (Bitplane) and Matlab software (Mathworks) were used for quantification of T cell speed and cell clustering. A threshold of 1 $\mu$ m between cell edges was used for quantification of cell-cell interactions, which account for low fluorescence frequently encountered at cell edges. An interaction was defined as 2 cells touching each other for at least 3 time points. The dwell time was defined as the half-life of interaction, which corresponds to the time for which 50% of the relevant interactions (OTI-OTI or OTI-NK) ended.

## **Statistical analysis.**

Comparisons between groups were analyzed with the t-test (fig.1A, 1C, 1E-J, 2F, 3G, 4I, 5D, 5F-I), one-way (fig.1B, 2C), or two-way ANOVA with multiple comparison (fig.1D, 4C, 4E-G, 5B), or Mantel-Cox test (fig.3F) using GraphPrism software. Data are mean + sem unless specified. Data were considered significant when P values were 0.05 or less. Ns=non-significant, \*P < 0.05, \*\*P < 0.001, \*\*\*P < 0.0002 and \*\*\*\*P < 0.0001.

## Contributions

A.G. and M.F.K. conceptualized the study and designed all experiments; J.N.M. performed all experiments unless specified; A.G. did *in vitro* experiments, 2-photon imaging and initial *in vivo* experiments; A.M.M and E.H contributed to immunochemistry, the *in vivo* CD8 T cell fate experiments and *in vivo* IFN $\gamma$ -production experiments; J.M.M performed immunohistochemistry and quantified CD8 T cell memory; L.F.K.U. performed experiments investigating endogenous responses. R.J.W. and Z.J.W. synthesized the fatty acid-modified oligonucleotides, advised on T cell labeling by fatty acid-modified oligonucleotides and wrote the fatty acid-modified oligonucleotides related methods and cartoon; A.G. and M.F.K. wrote the manuscript. A.G., J.N.M and M.F.K. revised the manuscript. All authors edited the manuscript.

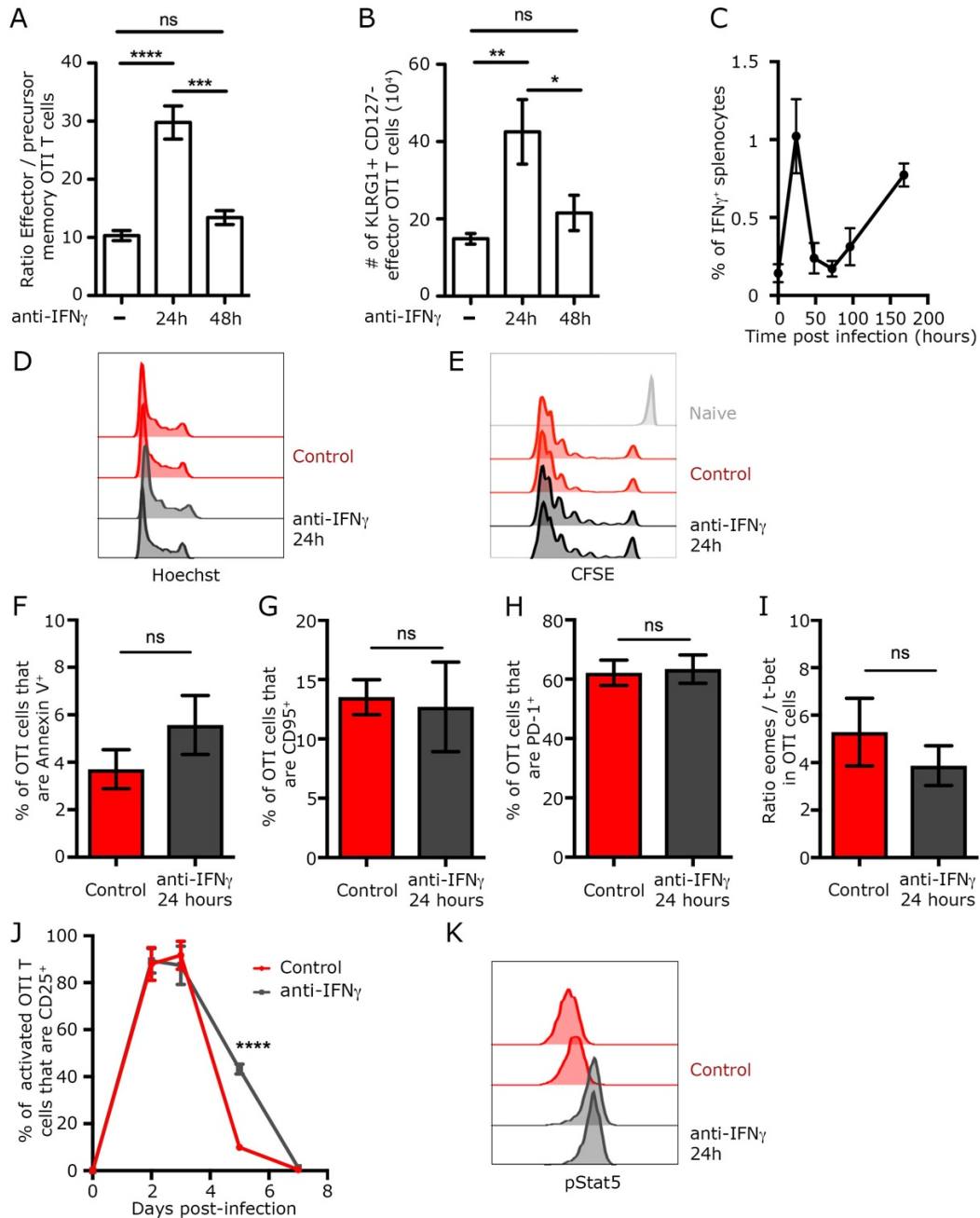


**Figure S1. Early IFN $\gamma$  production after LMOVA infection affects CD8 T cell differentiation through a non-canonical mechanism– Related to Figure 1.** (A-B) Mice transferred with OTI cells were infected with LMOVA. When indicated, mice (n=8) were treated with blocking IFN $\gamma$  Ab. The phenotype of OTI cells in the spleen was analyzed 10 days post-infection by flow cytometry using the antibodies CD8, CD45.1, KLRG1 and CD127. Effector cells were defined as KLRG1 $^+$ CD127 $^-$  and memory precursor cells as KLRG1 $^-$ CD127 $^+$ . Data are from three independent experiments. Data are mean with sem. ns=non-significant, \*P < 0.05, \*\*P < 0.001, \*\*\*P < 0.0002 and \*\*\*\*P < 0.0001 by one-way anova. **A**- Graph shows the ratio between effector and precursor memory OTI T cells. **B**- Graph shows the number of effector OTI T cells per 1/3 spleen. **C**- Mice were infected with LMOVA and treated with BFA 6 hours before being sacrificed. The percentage of live splenocytes expressing IFN $\gamma$  was analyzed by flow cytometry at the indicated times after infection. (**D-E**) Mice were transferred with CFSE-labeled OTI cells and infected with LM-OVA. When indicated, mice were treated with blocking IFN $\gamma$  Ab 24 hours post-infection. OTI cells in the spleen was analyzed 5 days post-infection, or over time (**J**) by flow cytometry. Histogram showing representative Hoechst stain (**D**), CFSE profile (**E**), Annexin V labeling (**F**), CD95 expression (**G**), PD-1 expression (**H**), t-bet/eomes ratio (**I**), CD25 expression (**L**) and Stat5 phosphorylation (**K**).



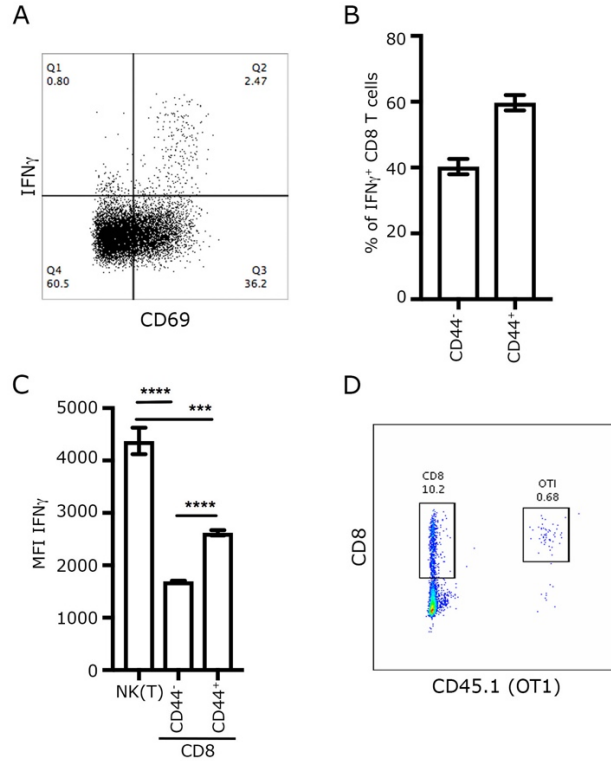


**Figure S2. Characterization of IFN $\gamma$  producing CD8 T cells and OTI T cells – Related to Figure 2.** (A-C) Mice were infected with LMOVA and treated with BFA 6 hours before being sacrificed. The CD8 T cell and NK cell populations among IFN $\gamma$  positive splenocytes 24 hours after infection were analyzed by flow cytometry using the antibodies NK1.1, CD8, CD69 and CD44. Data are from three independent experiments. **A**- Dot-plot shows CD69 and IFN $\gamma$  expression profile of CD8 T cells. **B**- Graph shows the percentage of IFN $\gamma$  expressing CD8 T cells that were CD44<sup>-</sup> and CD44<sup>+</sup>. **C**- Graph shows the IFN $\gamma$  Mean Fluorescence Intensity (MFI) of NK cells, CD44<sup>-</sup> CD8 T cells and CD44<sup>+</sup> CD8 T cells. Data are mean with sem. \*\*\* $P < 0.0002$  and \*\*\*\* $P < 0.0001$  by one-way anova. **D**- Mice were transferred with OTI CD45.1 T cells, infected with LMOVA and treated with BFA 6 hours before being sacrificed 24 hours after infection. Splenocytes were gated on IFN $\gamma$  positive cells, and the CD8 T cell and OTI T cell populations among those were analyzed by flow cytometry using the antibodies CD8 and CD45.1. Data are representative of two independent experiments.

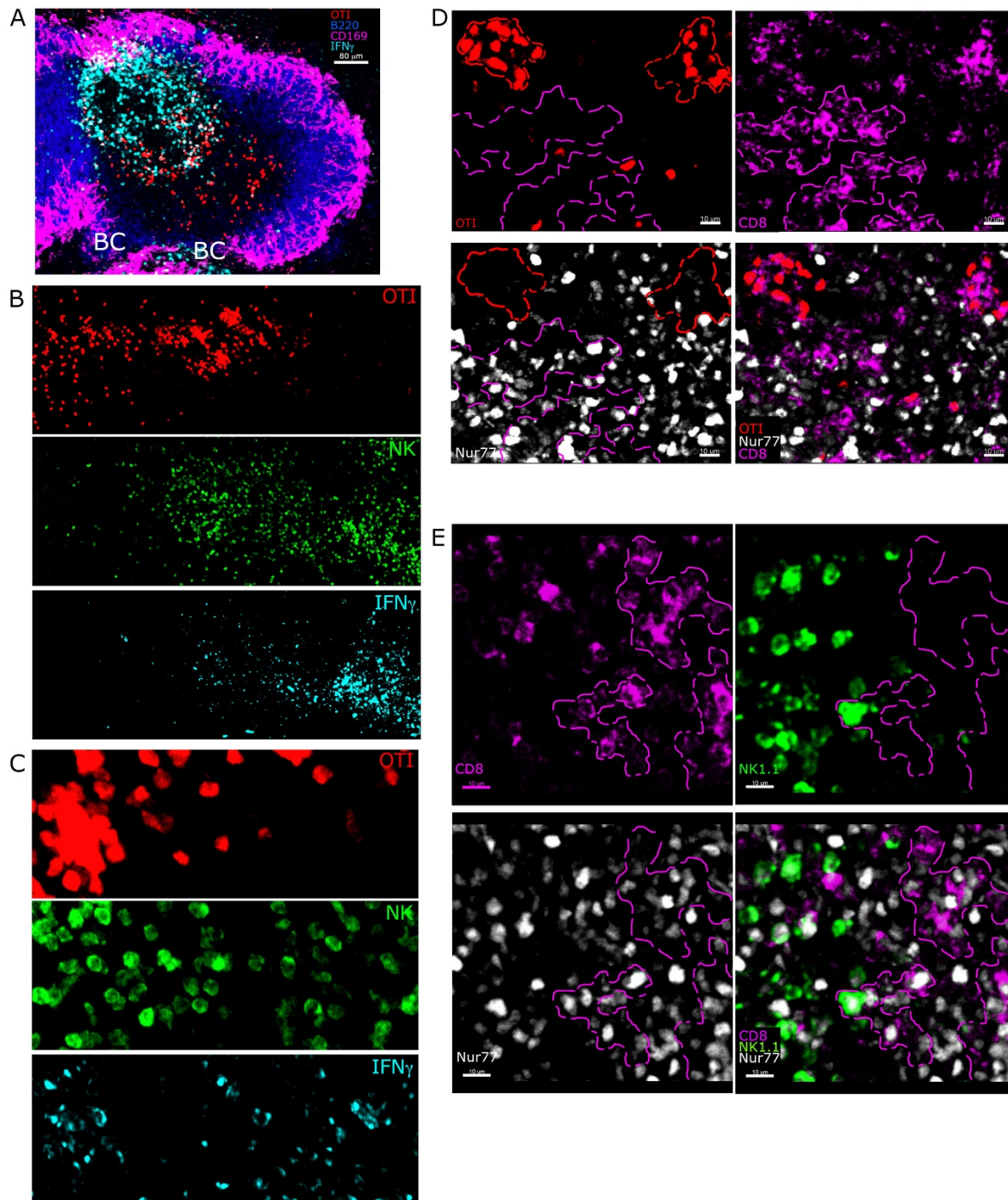


**Figure S3. Localization of IFN $\gamma$  producing cells and OTI T cells – Related to Figure 3.** A- Mice were transferred with CMTMR-labelled OTI cells, infected with LM-OVA and sacrificed 24 hours after infection. Spleen sections were stained for CD169 (magenta) to delineate the marginal zone, B220 (blue) to label B cell follicles and IFN $\gamma$  (cyan). Representative image of OTI (red) and IFN $\gamma$  producing cell localization in the white pulp. BC= Bridging Channel. (B-C) Single channels from image of Figure 3A and 3C, respectively. D- Nur77-GFP mice were transferred with CMTMR-labelled OTI cells, infected with LM-OVA and sacrificed 24 hours after infection. Spleen sections were stained for CD8 (purple) and GFP (white) to delineate activated endogenous CD8 T cells, and their location according to OTI T cells (red). OTI clusters and endogenous CD8 T cell cluster edges were delineated in magenta and green, respectively. E- Nur77-GFP mice were infected with LM-OVA and sacrificed 24 hours after infection. Spleen sections were stained for CD8 (magenta) and GFP (white) and NK1.1 (green) to delineate the location of NK cells according to activated endogenous CD8 T cell clusters. Endogenous CD8 T cell cluster edges were delineated in magenta.

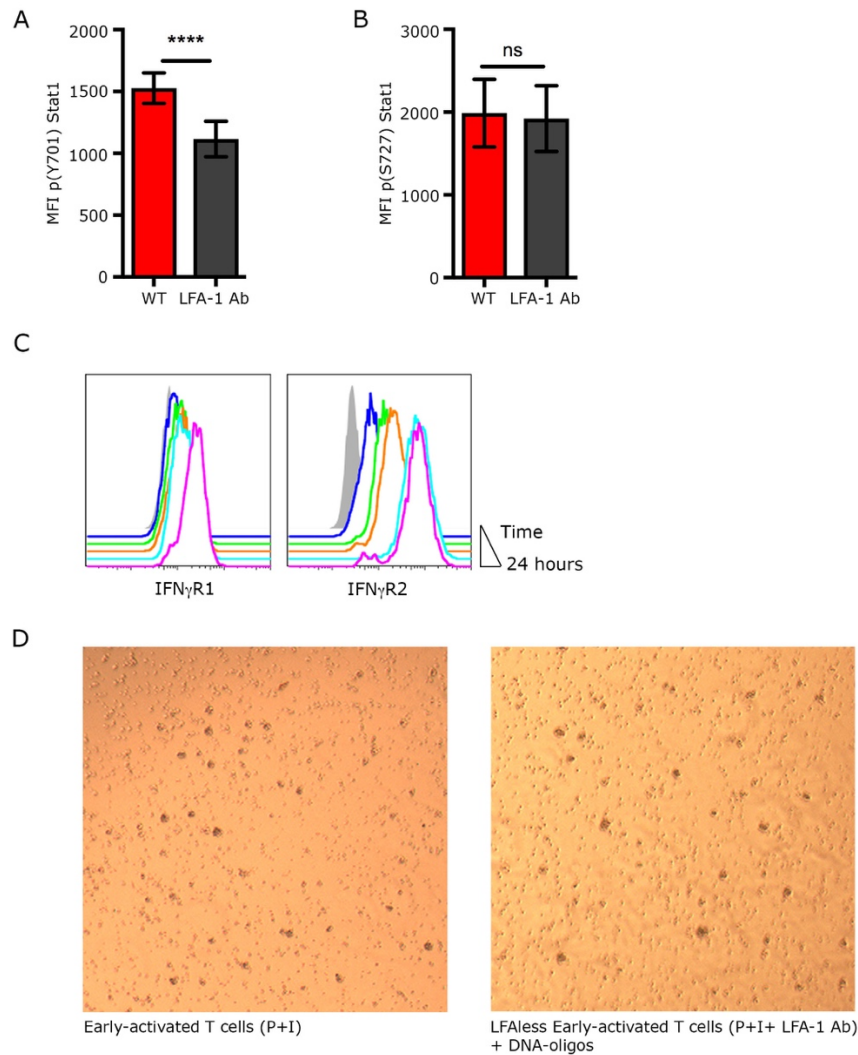


**Figure S4. Controls related to the contact-requirement for IFN $\gamma$  signaling in early-activated CD8 T cells – Related to Figure 4.** (A-B) OTI T cells were stimulated at low density with PMA and Ionomycin for 24 hours. Where indicated, cells were treated with LFA-1 blocking antibodies (LFA-1 Ab) or control antibodies (RatIgG2a) 5 hours before harvest. Stat1 phosphorylation on tyrosine 701 (A) and Serine 727 (B) was quantified by flow cytometry. Graph shows MFI. C- WT OTI T cells were stimulated at low density with PMA and Ionomycin for 24 hours. IFN $\gamma$ R1 (left) and IFN $\gamma$ R2 (right) surface expression was analyzed every 2 hours, the last time point being 24 hours after activation, by flow cytometry following acid stripping. D- IFN $\gamma$ <sup>-/-</sup> OTI T cells were stimulated at low density with PMA and Ionomycin for 24 hours. Cells were treated with LFA-1 blocking antibodies (“LFAless”), right panel) or control antibodies (RatIgG2a, left panel) 5 hours before harvest. Cells treated with LFA-1 blocking antibodies were forced to come in close proximity using oligonucleotides (DNA-Oligos) for 3 hours. Bright-field images show a typical example of cell behavior, showing equivalent cell clustering in both conditions.

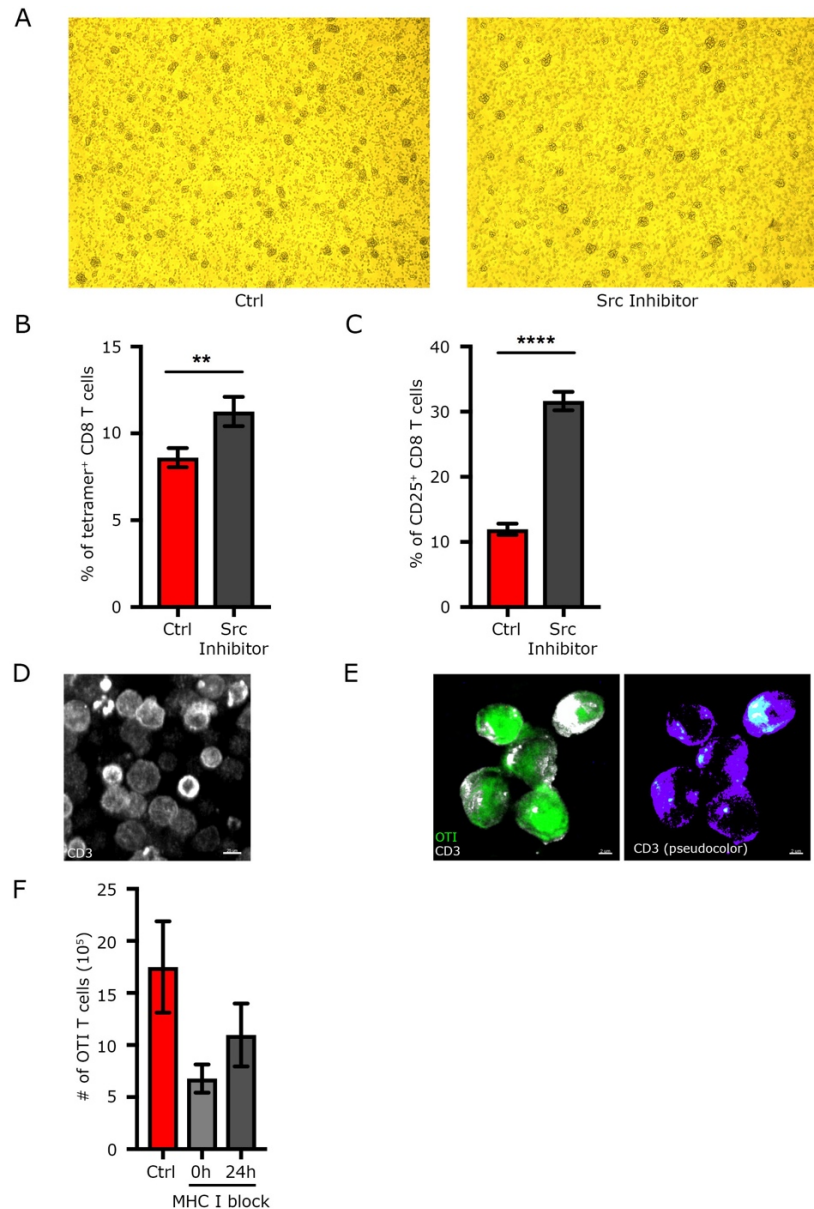


**Figure S5. Function of Src kinases during clustering events on endogenous CD8 T cell response following LMOVA infection – Related to Figure 5.** **A-** OTI T cells were stimulated with PMA and Ionomycin for 24 hours. When indicated, cells were treated with the Src inhibitor PP2 5 hours before harvest. Images show representative cell clustering at the time of harvest. **(B-C)** Mice were infected with LMOVA and treated with the Src inhibitor PP2 24 hours post infection when indicated. **B-** Frequency of cells positive for the SIINFEKL tetramer (OVA-specific endogenous cells) among CD8 T cells was analyzed 8 days after infection by flow cytometry. Data are from two independent experiments, n=15. **C-** Frequency of tetramer CD25 positive endogenous CD8 T was analyzed 5 days after infection by flow cytometry. Data are from two independent experiments, n=17. **D-** OTI T cells were stimulated with PMA and Ionomycin for 24 hours. Image shows representative staining with CD3 antibody in cell clusters. **E-** Mice were transferred with OTI-GFP cells, infected with LM-OVA and sacrificed 24 hours after infection. Spleen sections were stained for GFP and CD3. Picture is a representative example of CD3 localization (left: white; right: pseudocolor) on OTI cells (green). For clarity, CD3 stain has been masked to reveal only CD3 staining of OTI using Imaris. Scale bar, 2  $\mu$ m. **F-** Mice transferred with OTI T cells were infected with LMOVA and treated with MHC Class1 blocking antibody at the indicated time post infection. The number of OTI T cells among CD8 T cells was analyzed 8 days after infection by flow cytometry. Data are from two independent experiments, n=6.

**Movie S1.** 3-Dimensional representation of IFN $\gamma$  sub-localization in 2 interacting OTI cells – Image depicted in Figure 3D.

**Movie S2.** 3-Dimensional representation of IFN $\gamma$  sub-localization in NK cells – Image depicted in Figure 3D.

**Movie S3.** OTI cell and NK cell dynamics in the overlap region 24 hours post-infection – Related to Figure 3. NCR1-GFP<sup>+/-</sup> mice were transferred with  $1 \times 10^6$  CMTMR-labeled OTI and infected with  $10^4$  cfu LM-OVA. After 24 hours, spleen was explanted and OTI (red) and NK (green) cell behavior was determined by 2-photon microscopy. Movie shows a 15-minute time-lapse acquired in the OTI/NK overlap region. White arrows indicate T cell clustering.

**Movie S4.** Endogenous activated CD8 T cell dynamics 24 hours post-infection – Related to Figure 3. Nur77-GFP<sup>+/-</sup> mice were infected with  $10^4$  cfu LM-OVA. After 24 hours, spleen was explanted and stained for CD8 T cells. CD8 (red) and Nur77 (green) cell behavior was determined by 2-photon microscopy. Movie shows a 7-minute time-lapse.

## Supplemental Reference

1. Weber RJ, Liang SI, Selden NS, Desai TA, & Gartner ZJ (2014) Efficient targeting of fatty-acid modified oligonucleotides to live cell membranes through stepwise assembly. *Biomacromolecules* 15(12):4621-4626.